Role of Y94 in Proton and Hydride Transfers Catalyzed by Thymidylate Synthase†

Baoyu Hong,‡,§ Frank Maley,|| and Amnon Kohen*,‡

Department of Chemistry, University of Iowa, Iowa City, Iowa 52242, and Wadsworth Center, New York State Department of Health, Albany, New York 12201

Received July 11, 2007; Revised Manuscript Received September 26, 2007

ABSTRACT: Thymidylate synthase (TS) catalyzes the substitution of a carbon-bound proton in a uracil base by a methyl group to yield thymine in the de novo biosynthesis of this DNA base. The enzymatic mechanism involves making and breaking several covalent bonds. Traditionally, a conserved tyrosine (Y94 in *Escherichia coli*, Y146 in *Lactobacillus casei*, and Y135 in humans) was assumed to serve as the general base catalyzing the proton abstraction. That assumption was examined here by comparing the nature of the proton abstraction using wild-type (*wt*) *E. coli* TS (*ec*TS) and its Y94F mutant (with a turnover rate reduced by 2 orders of magnitude). A subsequent hydride transfer was also studied using the *wt* and Y94F. The physical nature of both H-transfer steps was examined by determining intrinsic kinetic isotope effects (KIEs). Surprisingly, the findings did not suggest a direct role for Y94 in the proton abstraction step. The effect of this mutation on the subsequent hydride transfer was examined by a comparison of the temperature dependency of the intrinsic KIE on both the *wt* and the mutant. The intrinsic KIEs for Y94F at physiological temperatures were slightly smaller than those for *wt* but, otherwise, were as temperature-independent, suggesting a perfectly preorganized reaction coordinate for both enzymes. At reduced temperatures, however, the KIE for the mutant increased with a decrease in temperature, indicating a poorly preorganized reaction coordinate. Other kinetic and structural properties were also compared, and the findings suggested that Y94 is part of a H-bond network that plays a critical role at a step between the proton and the hydride transfers, presumably the dissociation of H_4folate from the covalently bound intermediate. The possibility that no single residue serves as the general base in question but, rather, that the whole network of H-bonds at the active site catalyzes proton abstraction is discussed.

Thymidylate synthase (TS)[1] catalyzes the reductive methylation of 2′-deoxyuridylate (dUMP) with 5,10-methylene-5,6,7,8-tetrahydrofolate (CH_2H_4folate), forming thymidine monophosphate (dTMP) and 7,8-dihydrofolate (H_2folate) (*1*). TS activity is essential to living organisms since it catalyzes the de novo synthesis of one of the DNA building blocks. Consequently, TS is a common target in cancer chemotherapy, antibiotic drugs, and gene therapy (*2*, *3*). The TS-catalyzed reaction has been elucidated in detail by a wide variety of kinetic, genetic, and structural methodologies (*1*, *4*−*6*), which have shown that TS is a homodimer utilizing a half-of-the-sites-activity mechanism (*7*, *8*). Steady state measurements indicated a bi-bi ordered mechanism with substrate (dUMP) binding before the CH_2H_4folate (*4*, *9*). Kinetic and structural studies identified coherent protein motion that appears to be coupled to a hydride transfer step (*10*, *11*), which is rate-limiting for *wt* TS.

Scheme 1 illustrates the two main variations proposed for the chemical mechanisms along the complex cascade of TS catalysis. In the traditional proposed mechanism (*1*, *4*), E58 assists in the formation of an iminium ion (A in Scheme 1), which is subjected to nucleophilic attack by the C5 enolate of the C146-activated dUMP (*12*) to form a ternary intermediate (C). A proton is then abstracted from C5 of dUMP to form the enol D (step 4) (*4*). This is followed by the release of H_4folate from the ternary complex (step 5, E1CB mechanism) (*13*) which generates the exocyclic methylene intermediate (E). Finally, the product dTMP is formed in step 6 by transfer of a hydride from (6*S*)-H_4folate to the exocyclic methylene of the enzyme-bound nucleotide via a 1,3-S_N2 mechanism. Several experimental studies indicate that this last step is the overall rate-limiting step for both the first-order rate constant (k_{cat}) and the second-order rate constant (k_{cat}/K_M) (depicted below as V/K) (*10*, *14*, *15*). Recently, QM/MM calculations (*16*) suggested an alternative path with lower activation energies. In the new path, the keto−enol tautomerization at C4 of dUMP plays a minor role while the labile C6-S-Cys bond plays a major role. The differences from the traditional mechanism are as follows. (i) Steps 2 and 3 occur concertedly. (ii) The abstraction of the proton from C5 of dUMP involves E2 elimination of C146 (step 4′). (iii) The dissociation of CH_2H_4folate occurs

† This work was supported by NIH Grant R01 GM65368-01 and NSF Grant CHE-0133117 to A.K.

* To whom correspondence should be addressed. Telephone: (319) 335-0234. Fax: (319) 335-1270. E-mail: amnon-kohen@uiowa.edu.

‡ University of Iowa.

§ Current address: The Department of Pharmaceutical Chemistry, School of Pharmacy, University of California, San Francisco, CA 94158-2517.

|| New York State Department of Health.

[1] Abbreviations: TS, thymidylate synthase; KIE, kinetic isotope effect; RP-HPLC, reverse phase high-pressure liquid chromatography; LSC, liquid scintillation counter; dUMP and 5-FdUMP, 5-fluoro-2′-deoxyuridine 5′-monophosphate and 2′-deoxyuridine 5′-monophosphate, respectively; dTMP, 2′-deoxythymidine 5′-monophosphate; CH_2H_4-folate, N^5,N^{10}-methylene 5,6,7,8-tetrahydrofolate; H_2folate, 7,8-dihydrofolate; H_4folate, 5,6,7,8-tetrahydrofolate.

10.1021/bi701363s CCC: $37.00
Published on Web 11/14/2007

Scheme 1: Proposed Chemical Mechanisms of the TS-Catalyzed Reaction

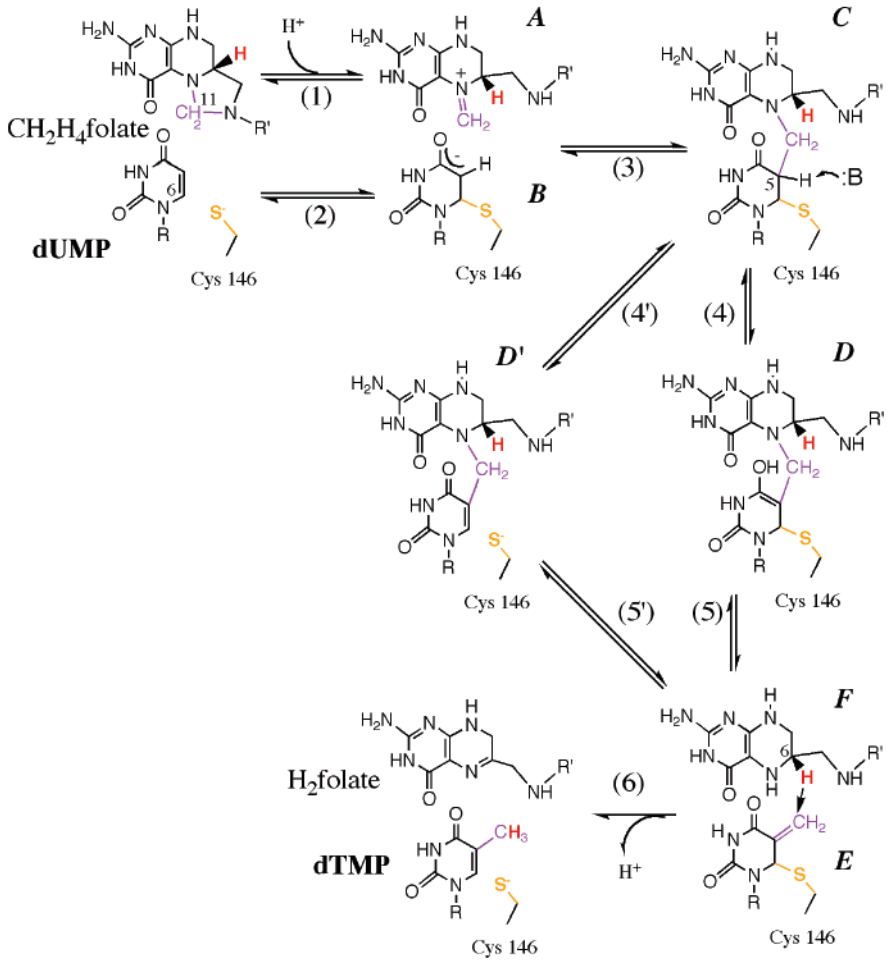

via 1,3-S_N2 substitution with the thiolate of C146 as the nucleophile and N5 of H_4folate as the leaving group (step 5′).

The abstraction of the proton from position 5 of the pyrimidine ring is crucial in the breakdown of the ternary intermediate and is the focus of this work. The general base in the active site has been proposed to be Y94 (see ref *4* and many references cited therein). Figure 1 presents the crystal structure of *wt Escherichia coli* TS with covalently bound dUMP and noncovalently bound folate analogue at the active site (PDB entry 2KCE). The water molecule (W608) is located 2.6 Å from the oxygen of Y94 and 3.6 Å from C5 of dUMP and was assumed to serve as the initial acceptor of the abstracted proton in step 5 (*4*, *13*, *17*−*19*). Hardy et al. (*20*) proposed that the general base in step 4 is N5 of the H_4folate through an "H-wire", using water as a conduit. Mutagenesis studies (*19*) demonstrated that several modifications of Y94 lead to loss of activity. This fact was interpreted as being support for a mechanism in which Y94 assists in the proton abstraction. These issues are further examined in this paper.

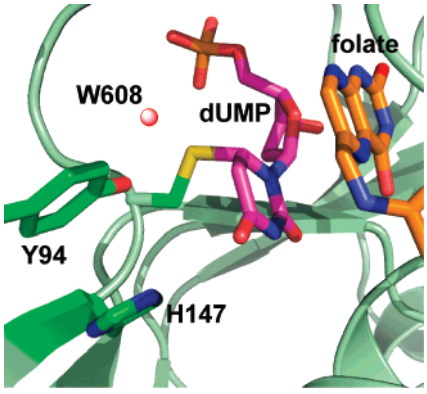

FIGURE 1: Structure of *wt E. coli* TS covalently bound to dUMP (PDB entry 2KCE) with Y94 and H147 highlighted in green, the water molecule closest to Y94 (1.7 Å) and to C5 of dUMP highlighted as a red sphere, the dUMP in magenta covalently bound to C146, and the pterin ring in orange.

Another interesting feature of this work is that no isotope effects have been measured on the C5−H bond cleavage, which is not a rate-limiting step for any measurable rate constant. Previous measurements monitored the ratio of ^3H to ^{14}C using [2-^{14}C,5-^{3}H]dUMP as a substrate with a saturating CH_2H_4folate concentration and reported no KIE (unity) or even a slightly inverse KIE (*4*). The reason for the inverse KIEs is likely to be a fast and reversible exchange of the C5 proton through steps 1−4, prior to the irreversible and rate-limiting hydride transfer in step 6. Furthermore, the high concentration of CH_2H_4folate, which binds after dUMP binds (*4*, *5*), would mask a possible intrinsic KIE if the isotopic label is on the substrate (*20*−*24*). In this work, the KIEs on this proton abstraction were studied as a function of the concentration of CH_2H_4folate in combination with the Northrop method (*25*−*28*). The observed KIEs versus the CH_2H_4folate concentration clearly indicated a kinetic mech-

anism with ordered substrate binding for the *wt* and less ordered binding for Y94F. A comparison of the intrinsic KIEs of the mutant and the *wt* served as a probe of the role of Y94 in this step.

Additionally, we investigated the effect of altering the hydrogen bond network at the active site via the Y94F mutation and the nature of another chemical transformation remote from Y94, namely the hydride transfer (step 6 in Scheme 1). The comparison of the temperature dependency of the intrinsic KIEs and activation parameters of Y94F with those of *wt* (*10*) indicated a minor effect of this mutation at physiological temperature, but a substantial distortion of the reaction's preorganization at reduced temperatures. Together, the examination of the effect of Y94F on the proton abstraction (step 4 or 4′) and on the hydride transfer (step 6) indicated that a more likely role of Y94 is in the protonation of N5 of H_4folate (the leaving group in step 5 or 5′), as discussed in detail below.

MATERIALS AND METHODS

Materials

[2-^{14}C]dUMP (specific radioactivity of 52 Ci/mol) and [5-^{3}H]dUMP (specific radioactivity of 13.6 Ci/mmol) were from Moravek Biochemicals. [^{2}H]$NaBH_4$ (>99.5% D) was from Cambridge Isotopes. [^{3}H]$NaBH_4$ (15 Ci/mmol) was from American Radiolabeled Chemicals. Dihydrofolate (H_2-folate) was synthesized by following the procedure of Blakley (*29*). [2-^{3}H]iPrOH was prepared by reduction of acetone with [^{3}H]$NaBH_4$ (specific radioactivity of 15 Ci/mmol) as described in detail elsewhere (*30*). All other materials were purchased from Sigma.

Synthesis of [2-^{14}C,5-D]dUMP (>99.5% D). [2-^{14}C,5-D]-dUMP was prepared by using a modification of the method of Wataya and Hayatsu (*31*−*33*) using L-cysteine in D_2O to catalyze H to D exchange at the C5 position of [2-^{14}C]dUMP. The reaction was conducted by incubation of [2-^{14}C]dUMP (~1 mM and 52 mCi/mmol) in a D_2O solution (>99.9% D) containing 1 M L-cysteine at 37 °C and a pD of 8.8 for 7 days. The reaction was carried out to completion as determined by ^{1}H NMR.

Synthesis of Isotopically C6 Labeled CH_2H_4folate for Measurement of a KIE on Hydride Transfer. The synthesis of (*R*)-[6-^{3}H]CH_2H_4folate was performed through a combination of two enzymatic reactions as described previously (*30*). Briefly, [2-^{3}H]iPrOH was prepared by reduction of acetone with [^{3}H]$NaBH_4$. $NADP^+$ was reduced by [2-^{3}H]iPrOH to (*R*)-[4-^{3}H]NADPH by alcohol dehydrogenase from *Thermoanaerobium brockii* (*tb*ADH). DHFR catalyzed the in situ conversion of H_2folate to (*S*)-[6-^{3}H]H_4folate using (*R*)-[4-^{3}H]NADPH, and then the isotopically labeled H_4folate was converted to (*R*)-[6-^{3}H]CH_2H_4folate upon quenching with formaldehyde. Similarly, the mixture of (*R*)-[6-^{3}H]CH_2H_4-folate and (*R*)-[6-^{2}H]CH_2H_4folate for the D/T KIE measurement was synthesized under the same conditions with the mixture of D- and T-labeled 2-propanols. The radioactively labeled CH_2H_4folate was purified by reverse phase HPLC, lyophilized, and stored at −80 °C prior to use.

Enzyme. Wild-type *E. coli* TS was prepared and purified according to the procedure of ref *34*. Y94F was prepared and purified as described in detail elsewhere (*6*, *13*). The mutant was stored as ammonium sulfate pellets at −80 °C and, prior to use, was dissolved and dialyzed against a mixture of 25 mM potassium phosphate, 10% ethylene glycol, and 2 mM DTT. *tb*ADH was purchased from Sigma.

Methods

Competitive and Intrinsic Primary Kinetic Isotope Effect (1° KIE) for C5 Proton Abstraction. The 1° KIEs on proton abstraction from the 5 position of the dUMP were measured competitively. The reaction mixture contained 50 mM β-mercaptoethanol, 1 mM EDTA, and 5 mM formaldehyde in 100 mM Tris buffer (pH 7.5). Prior to the kinetic assay, 1.5 Mdpm [5-^{3}H]dUMP, 0.5 Mdpm [2-^{14}C]dUMP, and varied concentrations of CH_2H_4folate (2−1000 μM) were added to the buffer mixture at 25 °C. The reaction was initiated by adding enzyme (*wt* or Y94F TS). Five aliquots of 100 μL were removed at different time points (t) and quenched with 30 μM 5-fluoro-2′-deoxyuridine 5′-monophosphate (F-dUMP, a nanomolar inhibitor of TS). Then, a concentrated solution of *wt* TS was added to the reaction mixture to a final concentration of 0.1 mM, followed by incubation for an additional 10 min to complete the reaction (t_∞). Two t_0 values (reaction mixture prior to adding enzyme and used as control) and three t_∞ values were obtained for each experiment, and independent experiments were performed in triplicate. All the quenched samples were stored in dry ice before HPLC analysis. The method of RP-HPLC separation and liquid scintillation counter (LSC) analysis of the ^{3}H/^{14}C ratio is described in detail elsewhere (*30*).

The competitive observed KIEs on the second-order rate constant V/K were determined using the following equation (*35*):

$$\mathrm{KIE} = \frac{\ln(1-f)}{\ln\left(1 - f\frac{R_t}{R_\infty}\right)} \quad (1)$$

where f is the fractional conversion to product dTMP (typically ranging from 20 to 80%) and R_t and R_∞ are ^{3}H/^{14}C ratios in products (water and dTMP) at each time point and time infinity, respectively. The fractional conversion f was calculated by

$$f = \frac{[^{14}\mathrm{C}]\mathrm{dTMP}}{[^{14}\mathrm{C}]\mathrm{dTMP} + [^{14}\mathrm{C}]\mathrm{dUMP}} \quad (2)$$

Figure 2 presents an example of measured H/T KIEs as function of f. Since the KIE on the proton abstraction has not been measured before, it is important to demonstrate that the KIE is reproducible in a series of independent experiments and that there is no upward or downward trends in the KIE as function of f.[2] Figure 3 presents the observed H/T KIEs of the mutant and the *wt* as a function of CH_2H_4-folate concentration. The analysis of the observed KIEs on the proton abstraction as function of CH_2H_4folate is presented in the Results and Discussion.

To determine the intrinsic KIE for this step, 5 μM CH_2H_4-folate was used to measure the observed H/T and D/T KIEs.

[2] Most artifacts in a competitive experiment will result in such a trend.

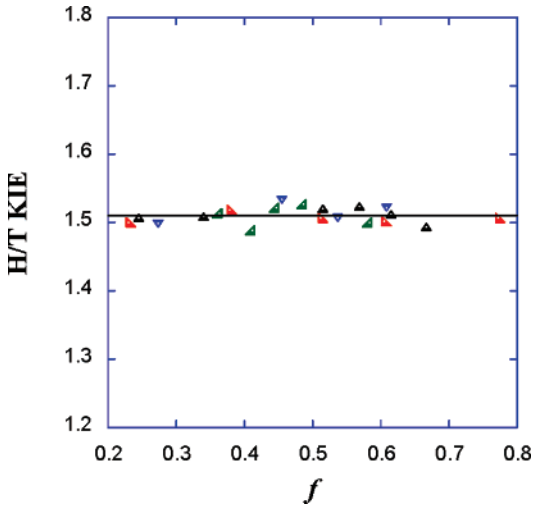

FIGURE 2: H/T KIEs as a function of fractional conversion as measured for *wt* TS at 25 °C in 5 μM CH_2H_4folate. The different colors and shapes represent points measured in four independent experiments. The average value is 1.52 ± 0.03, and no upward or downward trend is observed within statistical error.

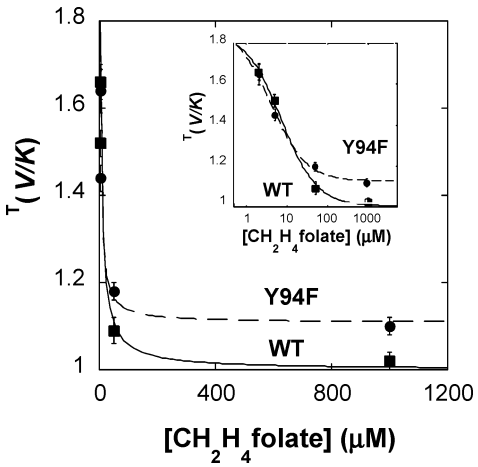

FIGURE 3: H/T KIE for proton abstraction as a function of CH_2H_4-folate concentration. Data with Y94F (●) and *wt* (■) are compared. Solid and dashed lines are fits to eq 5 for the *wt* and Y94F, respectively.

The observed D/T KIE was measured using the exact same conditions that were used for the H/T KIE except the [2-^{14}C]-dUMP was replaced with [2-^{14}C,5-D]dUMP. So, the ^{14}C now represents the D-transfer rather than H-transfer. Intrinsic KIEs are calculated from eq 3 (*25*−*28*):

$$\frac{{}^{T}(V/K)_{Hobs}{}^{-1} - 1}{{}^{T}(V/K)_{Dobs}{}^{-1} - 1} = \frac{k_T/k_H - 1}{(k_T/k_H)^{1/3.34} - 1} \qquad (3)$$

where ${}^{T}(V/K)_{H,obs}$ and ${}^{T}(V/K)_{D,obs}$ are the observed competitive H/T and D/T KIEs and k_T/k_H represents the reciprocal of k_H/k_T (intrinsic H/T KIE). Although the intrinsic H/T KIE is the only unknown in this equation, it cannot be solved analytically. Therefore, a program has been developed to solve this equation numerically (now available free of charge at http://cricket.chem.uiowa.edu/~kohen/tools.html). Since error propagations in this case cannot be conducted analytically from derivatization of eq 3, the intrinsic KIEs were analyzed by calculation the intrinsic KIEs from independent and random combinations of observed H/T and D/T KIEs (*36*). The Northrop method for a reversible step assumes a ${}^{T}K_{eq}$ close to unity (*25*−*27*). We measured the ${}^{D}K_{eq}$ using the Cys-activated dUMP as a model compound for intermediate C in Scheme 1 (as described in the following item) and found it to be unity within experimental error. Additionally, the ${}^{T}K_{eq}$ for the proton abstraction can be estimated to be close to unity from fractionation factors for protons bound to similar carbons, and the fractionation factor in the product water molecule being unity since water is the reference system (*37*). Finally, since the reverse step in question involves the competition of tritium and protons from water, as discussed below, even a larger EIE should have little effect on the outcome of the Northrop method.

Equilibrium Isotope Effect (EIE) on Activated dUMP. To assess the EIE (${}^{D}K_{eq}$) on the proton abstraction on C5 of dUMP, we used a model in which C6 is activated by a high concentration of Cys in solution. The activated complex was allowed to exchange with a 50% H_2O/D_2O mixture. Specifically, 270 mM dUMP and 1 M L-cysteine were incubated in a 50% (molar) H_2O/D_2O mixture at 37 °C and a pH of 8.8 for 5, 7, and 9 days. The progress of the exchange reaction was monitored by ^{1}H NMR until completion (no further change in H content at C5). For an accurate NMR examination, the samples were lyophilized and redissolved in pure D_2O at a pD of 1.5 (the exchange reaction does not proceed at this pD). Then, the ratio between the hydrogen on C6 (unexchangeable) and the one on C5 was determined by ^{1}H NMR. The hydrogen on C3′ was used as the integration reference of unity, and the H6/H5 ratio was determined in quintuplets. The H5/H6 values were 0.510 (±0.008)/1.010 (±0.007), indicating a ${}^{D}K_{eq}$ of 0.99 (±0.02) for the proton exchange with water.[3]

Competitive and Intrinsic Primary Kinetic Isotope Effect (1° KIE) on Hydride Transfer from C6 (Step 6 in Scheme 1). The competitive H/T and D/T KIEs for the hydride transfer from the 6 position of CH_2H_4folate with Y94F mutant were measured using the same conditions that were used with *wt* TS (*10*). In short, the reaction mixture contains 1.5 Mdpm tritiated (*R*)-[6-^{3}H]CH_2H_4folate for the H/T KIE or deuterated (*R*)-[6-^{2}H]CH_2H_4folate for the D/T KIE, 0.5 Mdpm [2-^{14}C]dUMP, 50 mM β-mercaptoethanol, 1 mM EDTA, and 5 mM formaldehyde in 100 mM Tris buffer at pH 7.5 (adjusted at each experimental temperature). An approximately 30% molar excess of dUMP was used in the reaction mixture to ensure 100% conversion of tritiated CH_2H_4folate at infinite time (essential for R_∞; see below). The reaction mixture was preincubated at the respective experimental temperatures and the reaction initiated by adding Y94F. At five different time points, 100 μL aliquots were removed and quenched with 30 μM F-dUMP. Concentrated *wt* TS was added to the reaction mixture to achieve 100% conversion (t_∞). Two t_0 values (used as quality control) and three t_∞ values were obtained for each experiment, and independent experiments were performed in at least duplicate. The competitive observed KIEs were determined by eq 1,

[3] A ${}^{D}K_{eq}$ of 1 would lead to a H5/H6 ratio of 0.5 so 0.5 × 1.01/0.51 = 0.99.

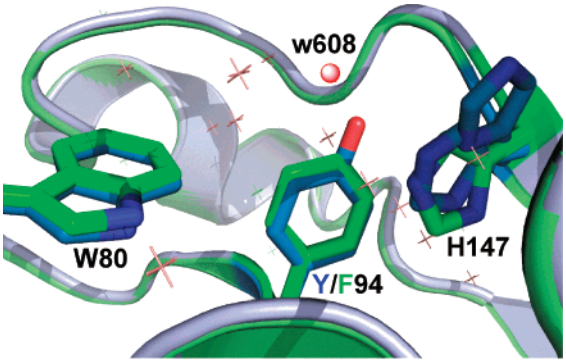

FIGURE 4: *wt* TS (blue, PDB entry 2FTQ) and Y94F (green, PDB entry 2FTN) with Y/F94, W80, and H147 presented as sticks. The water molecule closest to Y94 (w608, 2.6 Å from its O) is highlighted as a red sphere and is missing in the mutant. All other water molecules are marked by crosses and practically overlap for the *wt* and the mutant. See also Figure 3 in ref *38*. Note that the 2-fold orientation of H147 is only apparent in the *wt* (blue), but not in Y94F (green).

and the fractional conversion f was determined from eq 4 (*30*):

$$f = \frac{[^{14}\text{C}]\text{dTMP}}{(100 - \%_{\text{excess}})([^{14}\text{C}]\text{dTMP} + [^{14}\text{C}]\text{dUMP})} \quad (4)$$

where % excess = [(total ^{14}C) − ([2-^{14}C]dTMP)$_\infty$]/(total ^{14}C).

The intrinsic H/T and D/T KIEs are calculated from eq 3 with the error propagation processed in the same way that was used for the aforementioned proton abstraction step. The analysis of these data is described in the Results and Discussion.

Steady State Kinetics. The initial velocities were measured under steady state conditions in a buffer mixture containing 50 mM DTT, 5 mM formaldehyde, 1 mM EDTA, and 100 mM Tris at pH 7.5 (adjusted at each experimental temperature). The reaction was monitored by following the increase of absorbance at 340 nm upon conversion of CH_2H_4folate to H_2folate ($\Delta\epsilon_{340}$ = 6.4 mM^{-1} cm^{-1}) (*14*). The individual reaction mixture was pre-equilibrated at experimental temperatures and initiated by adding enzyme. Each measurement was conducted in at least duplicate, and the data were analyzed as described in the Results and Discussion.

RESULTS AND DISCUSSION

Structural Comparison

A recent X-ray crystallography study (*38*) examined the Y94F mutant at 1.6 and 2.0 Å resolution (without and with ligands, respectively). An overlap of crystal structures of the *wt* and the mutant (Figure 4) indicates a perfect overlap, including electron density for defined water molecules [rmsd = 0.014 Å (*38*)]. The obvious exception is the lack of the hydroxyl at residue 94 and the water molecule that is hydrogen bonded to the OH group in the *wt*. In the *wt* enzyme, Y94 is part of a H-bond network containing water molecules, H147, C146, and N5 of H_4folate. In Y94F, there is no electron density at the locations of the mutated hydroxyl and water 608. It is suggested that delocalized water molecules now occupy that space. It is also apparent that H147 in the *wt* has more than one conformation (from partial electron density), while Y94F adopts only a single conformation. This is the most substantial effect on the whole network of H-bonding at the active site.

Scheme 2: Binding Scheme for a Sequential Mechanism[a]

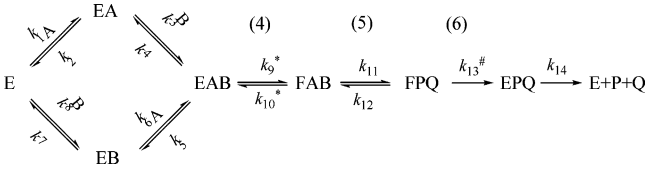

[a] In this case, A represents dUMP and B represents CH_2H_4folate. The relevant steps from Scheme 1 are presented in parentheses. Rate constants that are isotopically sensitive in the proton abstraction experiments (using labeled dUMP) are marked with an asterisk, and the one that is isotopically sensitive in the hydride transfer experiments (using labeled CH_2H_4folate) is marked with a number sign.

Proton Abstraction

The substrate dUMP, labeled with tritium at C5, is commonly used to measure the enzyme's activity (*4*). The use of release of tritium from [5-^{3}H]dUMP to measure the reaction rate relies on the assumption that there is no effective (observed) KIE on that step. This assumption is substantiated by the fact that the proton abstraction is not rate-limiting in the overall reaction (*4*, *10*) and by the ordered nature of the *wt* TS reaction. The intrinsic KIE of step 5 in Scheme 1 has never been measured before (to the best of our knowledge). Previous experiments that monitored the ^{3}H/^{14}C ratio in the mixture of [5-^{3}H]dUMP and [2-^{14}C]dUMP (*4*, *24*) reported KIEs close to unity. This is probably due to the ordered binding mechanism of the *wt* TS (*1*) that "masked" the KIE when the labeling was on the dUMP that binds first (*21*, *39*, *40*). The relationship between the observed KIE on the second-order rate constant $^T(V/K)$ and the KIE after the formation of the ternary complex ($^Tk_9$ in Scheme 2) is described in eq 5 (*21*, *27*, *41*):

$$^{\text{T}}(V/K) = \frac{^{\text{T}}k_9 + C_\text{f} + C_\text{r}\,^{\text{T}}K_\text{eq}}{1 + C_\text{f} + C_\text{r}} \quad (5)$$

where k_n values are the microscopic rate constants for the kinetic steps described in Scheme 2, C_r is the reverse commitment, which in the case of the current experiments is close to zero.[4] $^TK_{eq}$ is the equilibrium isotope effect on the proton abstraction, which is expected to be close to unity.

The forward commitment C_f is described by eq 6:

$$C_\text{f} = \frac{k_9}{k_5 + \dfrac{k_2 k_4}{k_2 + k_3[\text{B}]}} \quad (6)$$

where [B] is the concentration of the second substrate

[4] The reverse commitment is defined as $C_r = k_{10}/k_{11} + k_{10}k_{12}/k_{11}k_{13}$. Since C5 of dUMP is only trace labeled with tritium, k_{10} effectively represents competition between the water protons and the trace tritium. For the sake of simplicity, we follow the precedence of previous studies using [5-^{3}H]dUMP (*4*) and assume that the effective k_{10} is close to zero and thus C_r can be ignored in most of the following discussion. This assumption is further supported by comparison of the observed KIE at zero B concentration (1.8; see Figure 2) with the intrinsic KIE ($^Tk_9$ = 3.2 as calculated below). The combined commitment is only 0.45, leaving little apparent contribution for C_r alone. At any rate, C_r is independent of [B] and does not affect the conclusion regarding the effect of the mutation on the reaction order.

Table 1: Kinetic Isotope Effect of the Wild-Type and Y94F TS on Proton Abstraction at 25 °C

KIE	wild type	Y94F
$^{T}(V/K)_{H}$[a]	1.52 ± 0.03	1.44 ± 0.03
$^{T}(V/K)_{D}$[a]	1.17 ± 0.01	1.15 ± 0.01
H/T KIE_{int}	3.2 ± 0.2	3.2 ± 0.3
D/T KIE_{int}	1.41 ± 0.03	1.42 ± 0.04
H/D KIE_{int}	2.2 ± 0.1	2.3 ± 0.2

[a] At 5 μM CH_2H_4folate.

(CH_2H_4folate in this case). Apparent from eqs 5 and 6 is the fact that the observed $^{T}(V/K)$ is dependent on the concentration of B, and its observed value can change between two finite values [C_f changes from k_9/k_5 to $k_9/(k_5+ k_4)$ as [B] changes from infinity to zero]. In contrast to the random mechanism, the C_f in an ordered mechanism in which A binds first follows

$$C_f = \frac{k_9}{k_4} + \frac{k_3[B]}{k_2 k_4} \quad (7)$$

In this case, the observed $^{T}(V/K)$ is dependent on the concentration of B, and its observed value can change from unity (no KIE) to a finite value [C_f changes from infinity to k_9/k_4 as [B] changes from infinity to zero (*21*)].

In this study, the observed KIEs on the abstraction of the proton from C5 of dUMP were measured as a function of the CH_2H_4folate concentration to ascertain the kinetic mechanism for *wt* TS and Y94F. Figure 3 presents the observed KIEs as a function of CH_2H_4folate concentration. The observation that the observed H/T KIE for the *wt* approaches unity at high concentration of CH_2H_4folate (1.02 ± 0.02 at 1 mM CH_2H_4folate) while Y94F goes to an asymptote at a finite value (1.10 ± 0.02) indicates that the *wt* binding mechanism is strictly ordered [within experimental error and in agreement with previous studies (*1*)], but that of the mutant is more random (*21*). Also, the observed KIEs for the *wt* and Y94F are similar at zero B concentration [1.86 ± 0.10 and 1.96 ± 0.15, respectively (Figure 3)]. This last observation, together with the intrinsic KIEs (see below), indicates a similar commitment on $^{T}(V/K)$ for the *wt* and the mutant.

To access the intrinsic KIE on the proton transfer step, we measured the D/T KIE at a low CH_2H_4folate concentration and then assessed the intrinsic KIE using the Northrop method (*25*−*27*). A concentration of 5 μM CH_2H_4folate was used to ensure sufficient conversion of radioactively labeled dUMP on one hand and large observed KIE values (small relative error) due to a small commitment on the other hand. The intrinsic H/T KIEs on the proton abstraction for the *wt* and Y94F are practically the same [3.25 ± 0.31 and 3.17 ± 0.22, respectively (Table 1)].[5]

Summary of the Proton Abstraction Step (Step 4 or 4′ in Scheme 1)

An intrinsic KIE of the abstraction of the proton from C5 of dUMP is determined here for the first time. The intrinsic KIEs for both the mutant and the *wt* are similar ($^{T}k \approx 3.2$), suggesting that the effect of the Y94 mutation on this transformation was too small to be detected. Apparently, while the Y94F mutation reduced the order of binding by increasing the rate of release of dUMP from the ternary complex (k_5), it did not affect the actual proton transfer step. Apparent from Figure 3 is the fact that the level of kinetic complexity that masks the intrinsic KIE ($^{T}k_9$) on the second-order rate constant $^{T}(V/K)$ at zero CH_2H_4fole appears to be small and similar for both *wt* and the mutant ($C \approx 0.45$).[6]

The relatively small intrinsic KIE is in accordance with a preactivated C5−H bond and an asymmetric transition state for this transformation (*35*). QM/MM calculations (via collaboration with Moliner and co-workers) aimed at quantitatively examining this observation are underway.

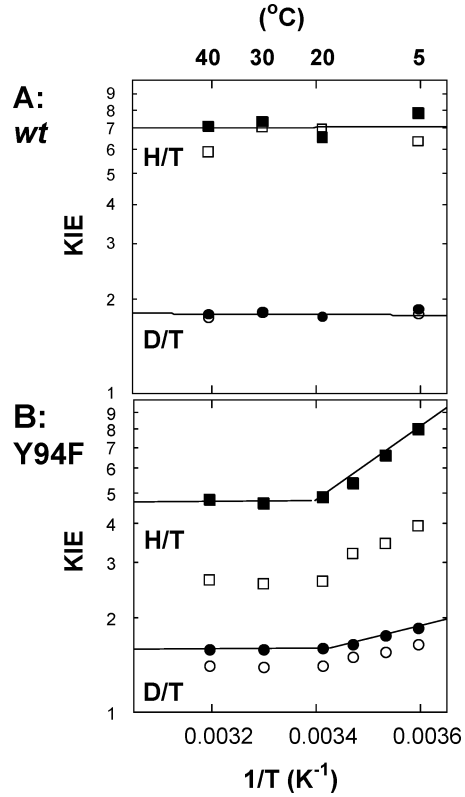

FIGURE 5: Arrhenius plots of observed (white symbols) and intrinsic (black symbols) primary H/T KIEs (squares) and primary D/T KIEs (circles). The lines are the exponential fittings of the intrinsic KIEs to eq 4: (A) *wt* and (B) Y94F.

Hydride Transfer

The intrinsic KIEs on the hydride transfer step (step 6 in Scheme 1) were measured and compared with those of the *wt* using CH_2H_4folate labeled with H, D, or T at its *R*-C6 position as described in ref *10*. Since in this part, only the hydride was isotopically labeled, all the other kinetic steps are not isotopically sensitive and the kinetic equations used are not different from those used for any other system with a single isotopically sensitive step. Figure 5 shows both the temperature dependence of the observed and intrinsic KIEs of the *wt* and Y94F. The analysis of the temperature

[5] With zero B, C_f equals k_9/k_4 for the *wt* and $k_9/(k_5 + k_4)$ for the mutant (see eq 6). Since C_f can also be calculated using the independently measured intrinsic KIE, it is tempting to calculate all the microscopic rate constants in Scheme 2. However, k_4 and k_9 do not have to be the same for both enzymes, and k_9 is likely to be much faster in the *wt*. Consequently, the current data are insufficient for extraction of all the microscopic rate constants.

[6] Where $C = C_f + C_r$ and $^{T}K_{eq}$ is close to unity.

Table 2: Rates and Isotope Effects on Arrhenius Parameters of the Wild-Type and Y94F TS on Hydride Transfer[a]

	wild type[b]	Y94F		
	5−40 °C	5−20 °C	20−40 °C	SC A_L/A_T[c]
A_H/A_T	6.9 ± 1.0	0.0002 ± 0.0001	4.5 ± 0.5	0.5−1.6
A_D/A_T	1.8 ± 0.1	0.07 ± 0.02	1.6 ± 0.1	0.9−1.2
ΔE_{aH-T}	0.02 ± 0.09	6.0 ± 0.5	0.03 ± 0.40	
ΔE_{aD-T}	0.01 ± 0.02	1.8 ± 0.2	0.06 ± 0.12	
E_a	4.0 ± 0.3	6.2 ± 0.3	3.1 ± 0.1	
$\Delta H^{\ddagger}$	3.4 ± 0.08	5.6 ± 0.3	2.5 ± 0.1	
$T\Delta S^{\ddagger}_{25\,°C}$	−13.7 ± 0.7	−14.5 ± 0.5	−17.6 ± 0.7	

[a] All energy units are kilocalories per mole. [b] From ref *10*. [c] Semiclassical limits of isotope effects on the preexponential factor of the Arrhenius equation (*35*, *45*, *46*, *53*).

dependence of intrinsic KIEs proceeded by exponential fitting of the data to the Arrhenius equation for KIEs:

$$k_L/k_T = A_L/A_T \exp[(E_T - E_L)/RT] \quad (8)$$

where k_L/k_T is the L/T KIE with L representing the light isotopes, A_L/A_T is the isotope effect on preexponential factors, and $E_T - E_L$ is the isotope effect on activation energy. The biphasic behavior of the intrinsic KIEs for the mutant (Figure 5B) suggested an intrinsic phase transition (*42*, *43*), so the data were fitted in temperature ranges of 40−20 and 20−5 °C independently. Above 20 °C, the KIE was temperature-independent ($E_T - E_H = -0.03 \pm 0.30$ kcal/mol), and the ratios of the Arrhenius preexponential factors (Table 2) are well above the semiclassical values (*44*−*46*). In the lower temperature range, the KIEs were temperature-dependent and the KIEs on the Arrhenius preexponential factors were inverse ($A_H/A_T < 1$) and below the semiclassical limits (Table 2).

Whether the temperature dependence of the KIEs can be understood within the framework of tunneling correction to transition state theory (*35*, *45*) depends on the assessment of the activation parameters on the reaction rate. To assess the activation parameters for the hydride transfer step in the high and low temperature ranges, it is necessary to extract the rates of that chemical step ($k_{hydride}$) in each temperature range. We used the method developed by Klinman and coworkers (*47*, *48*):

$$k_{hydride} = \frac{k_{cat}({}^{D}k - 1)}{{}^{D}k_{cat} - 1} \quad (9)$$

where $k_{hydride}$ is the unknown rate of the hydride transfer step, ${}^{D}k$ is the intrinsic H/D KIE for this step at each temperature (see Figure 5B), and ${}^{D}k_{cat}$ is the H/D KIE for k_{cat} using C6-labeled CH_2H_4folate. To assess the activation parameters for the two temperature regimes, k_{cat} was measured at 5, 20, and 40 °C, and eq 9 was used to assess $k_{hydride}$ (Table 3). The Arrhenius equation was used to calculate E_a for the physiological and low temperature ranges [3.1 and 6.2 kcal/mol, respectively (Table 2)].

The activation energy in the physiological temperature range, together with the temperature-independent intrinsic KIEs, suggested that, as with the *wt*, a Marcus-like model (*46*, *49*−*52*) is needed to explain the findings for Y94F (*10*). In such a model, the rate for hydrogen tunneling arises from the combination of two terms: one is nonisotopically sensitive but determines most of the temperature dependence of the rates, and the other [depicted as the Franck−Condon term (*49*)] is isotopically sensitive and includes a tunneling contribution and classical fluctuations between the donor and acceptor. The tunneling in such a model is dominated by the symmetry of the vibration levels (reorganization energy λ and driving force $\Delta G°$, the mentioned "rearrangement" term in Marcus theory) and by the fluctuations of the distance between the donor and acceptor (termed "gating") (*49*, *51*). According to the Marcus-like model, the lack of temperature dependence for both *wt* and Y94F in the higher temperature range indicates ideal prearrangement of the donor and acceptor prior to tunneling, which eliminates the effect of thermally activated gating. The comparison of Y94F to the *wt* suggests that the hydride transfer for both proceeds with a similar "environmentally coupled tunneling" (*50*) in the physiological temperature range. However, at lower temperatures, the increase in the Y94F activation energy relative to that of the *wt* ($\Delta E_{aY94-wt}$ is ∼2.8 kcal/mol) suggests a poorly preorganized reaction coordinate and substantial need for gating (*46*, *49*, *50*).

Table 3: Observed k_{cat} and ${}^{T}k_{cat}$ Values Used To Assess the Values of $k_{hydride}$ at 5, 20, and 40 °C Using eq 9[a]

	wild type[b]		Y94F	
temp (°C)	k_{cat} (s^{-1})	k_{cat} (s^{-1})	${}^{D}k_{cat}$	$k_{hydride}$ (s^{-1})
40	1.6	0.0067	2.24	0.0109
20	1.1	0.0055	2.36	0.0080
5	0.73	0.0023	4.20	0.0026

[a] All relative errors are <2% of the measured values and <6% of the calculated $k_{hydride}$. [b] From ref *10*.

Examination of the activation parameters in Table 2 results in an interesting observation: Most of the reduction in activity caused by the mutation appears to be on the entropy of activation ($\Delta T\Delta S^{\ddagger}$). The change in the enthalpy of activation, $\Delta\Delta H^{\ddagger}$, was estimated to be 0.9 kcal/mol, while $-\Delta T\Delta S^{\ddagger}$ was ∼3.9 kcal/mol at 25 °C. Similar results were also observed for mutants of dihydrofolate reductase (*36*), but it is not clear at this stage how general this phenomenon is. We hope that attracting the community's attention to these observations will lead to more data collection addressing the effect of mutations on activation parameters, and maybe to a better rationalization of this phenomenon.

The relationship between the observed and intrinsic KIEs can be extracted from eq 5 (*27*, *46*). At 20 °C, the observed H/T KIE on *V*/*K* of Y94F was measured to be 2.62 ± 0.01, while the intrinsic value is 4.86 ± 0.18, resulting in a commitment of 1.39 for the hydride transfer step. By contrast, the hydride transfer in the *wt* is commitment-free (commitment close to zero) at room temperatures (*10*). The inflated commitment of the observed KIE on *V*/*K* for Y94F indicates that this hydride transfer step is no longer commitment-free (rate-limiting) and that a preceding step becomes rate-limiting for this mutant.

Summary of the Hydride Transfer Step (Step 6 in Scheme 1)

Y94F exhibits biphasic behavior, with temperature-independent KIEs at physiological temperature and a steep temperature dependency under 20 °C (Figure 5). At physiological temperatures, the intrinsic KIEs were as temperature

independent as those of the *wt*. This is in accordance with conservation of the internal dynamics and coupling of the environment to the hydride transfer step (*46*, *50*), indicating only a minor role for Y94 in step 6. At reduced temperatures, the substantial temperature dependency of the KIEs with Y94F indicates a poorly preorganized reaction coordinate and a need for thermal gating of the donor−acceptor distance (*46*, *50*).

The phenomenon of the intrinsic phase transition of this type has been previously reported for thermophilic enzymes (*42*, *43*, *46*) but not yet for a mesophilic enzyme. A possible explanation for the phase transition at 20 °C for Y94F (Figure 5) is that the removal of the "anchored" Tyr94 hydroxyl and the lack of localization of the water molecule closest to C5 of dUMP (red sphere in Figure 4) disrupt the H-bond network at the active site. This, in turn, may alter the structural and dynamic properties of that network (which serves as the acceptor for the C5 proton), leading to a poorly preorganized reaction coordinate and a longer effective donor−acceptor distance at reduced temperatures (*46*, *50*).

Kinetic Analysis: Which Step(s) Is Affected by the Y94F Mutation?

Observations. (1) Hydride transfer is rate-limiting for both V/K and k_{cat} in the *wt* (the commitments on both rate constants are close to zero). In contrast, for Y94F, both k_{cat} and V/K for dUMP are masked (the observed KIEs are smaller than the intrinsic KIEs due to non-zero commitment). This indicates that the mutation affects a kinetic step that is part of both rate constants; e.g., the affected kinetic step is between the formation of the ternary complex and the first irreversible step. Specifically, (a) for Y94F, the inflated commitment (relative to that of the *wt*) for the hydride transfer's $^{T}(V/K)$ indicates that the step affected by mutation precedes the hydride transfer. (b) For Y94F, there is a small difference in commitment for the second-order rate constant $^{T}(V/K)$ of proton transfer, which indicates a small effect of mutation on the preceding steps, suggesting that most of the effect is after the proton abstraction.

(2) The intrinsic KIEs for the proton transfer (using [5-^{3}H]-dUMP) are the same for the *wt* and Y94F. This result suggests that the mutation does not affect the proton abstraction step per se.

(3) The K_M for dUMP is not affected by mutation, but the K_M for CH_2H_4folate is increased (*19*). This is in accordance with random binding for the mutant, which is proposed here on the basis of the dependence of the observed KIEs for proton abstraction on CH_2H_4folate concentration.

(4) Santi, Schultz, and co-workers (*19*) examined relevant mutants (Y146 in *L. casei* TS) as catalysts for CH_2H_4folate-independent dehalogenation of [5-Br]dUMP, a reaction which simulates early steps of the normal pathway up to and including formation of an enzyme−nucleotide covalent adduct. Many of these mutants had activity comparable to that of the *wt* enzyme, indicating that the effects of the mutations occur after the initial covalent adduct is formed.

Interpretation. The effect of the mutation on steps that precede the formation of the ternary complex and proton abstraction is small and mostly reflects the reduced binding capacity of dUMP (larger k_5 in Scheme 2). Most of the effect is on a step(s) that take place between the two H-transfer steps, specifically step 5 or 5′ in Scheme 1. Possible events that may occur along step 5 are deprotonation of the enolate in C4 and protonation of N5 of the H_4folate leaving group. Possible events that may occur along step 5′ are deprotonation of the thiol (if protonated during the elimination step 4′) and protonation of N5 of the H_4folate leaving group.

CONCLUSIONS

New insight into the chemical mechanism of the thymidylate synthase-catalyzed reaction is presented. Many studies have proposed that a conserved active site tyrosine (Y94 in *ec*TS) serves as a general base that enhances proton abstraction during the elimination of H_4folate (step 4 in Scheme 1; for a review, see ref *4*). The effect of the Y94F mutation on two distinct chemical steps has been examined. These steps were the proton abstraction step (step 4 in Scheme 1) and the hydride transfer step (step 6 in Scheme 1). The findings indicate that the proposed tyrosine (Y94, 3.6 Å from the proton donor) is not the main contributor to the proton abstraction step, but rather the whole network of H-bonds at the active site appears to serve as the general base. This conclusion is in accordance with the proposal of Hardy and co-workers (*20*), who used 5-deazatetrahydrofolate and concluded that N5 of H_4folate contributes to this general base. Additional candidates away from C5 are the imidazole and carboxylate side chains of H147 (5−6 Å) and E58 (∼7 Å). Out of these, we prefer the closer and more basic imidazole group. Future work will examine the H147V mutant and the *wt* TS from *Bacillus subtilis*, which has a Val rather than His in that position. It is of course possible that no single functional group exclusively constitutes the general base, but all three contribute to the basicity of the initial proton acceptor (a water oxygen).

What accounts for the 2 order of magnitude decrease in Y94F activity relative to that of *wt* TS? Taken together, the findings suggest that at physiological temperature the step most affected by the mutation occurs after the proton abstraction and prior to the hydride transfer. According to the mechanism illustrated in Scheme 1, this is likely to be step 5 or 5′, the protonation of N5 of H_4folate (in both paths) or the deprotonation of the enol in step 5, respectively. Additionally, the mutation weakens the binding and enhances the release of dUMP, which results in a random binding sequence (Scheme 2). QM/MM calculations comparing this mutant to the *wt* (*16*) are underway and may offer a molecular insight into the findings reported here.

ACKNOWLEDGMENT

We are grateful to Drs. Judith Klinman, Paul Cook, and Dexter Northrop for fruitful and helpful discussions.

REFERENCES

1. Carreras, C. W., and Santi, D. V. (1995) The catalytic mechanism and structure of thymidylate synthase, *Annu. Rev. Biochem. 64*, 721−762.
2. Phan, J., Steadman, D. J., Koli, S., Ding, W. C., Minor, W., Dunlap, R. B., Berger, S. H., and Lebioda, L. (2001) Structure of human thymidylate synthase suggests advantages of chemotherapy with noncompetitive inhibitors, *J. Biol. Chem. 276*, 14170−14177.
3. Sergeeva, O. A., Khambatta, H. G., Cathers, B. E., and Sergeeva, M. V. (2003) Kinetic properties of human thymidylate synthase, an anticancer drug target, *Biochem. Biophys. Res. Commun. 307*, 297−300.

4. Finer-Moore, J. S., Santi, D. V., and Stroud, R. M. (2003) Lessons and conclusions from dissecting the mechanism of a bisubstrate enzyme: Thymidylate synthase mutagenesis, function, and structure, *Biochemistry 42*, 248−256.
5. Stroud, R. M., and Finer-Moore, J. S. (2003) Conformational dynamics along an enzymatic reaction pathway: Thymidyate synthase, "the movie", *Biochemistry 42*, 239−247.
6. Saxl, R. L., Reston, J., Nie, Z., Kalman, T. I., and Maley, F. (2003) Modification of *Escherichia coli* thymidylate synthase at tyrosine-94 by 5-imidazolylpropynyl-2′-deoxyuridine 5′-monophosphate, *Biochemistry 42*, 4544−4551.
7. Maley, F., Pedersen-Lane, J., and Changchien, L. (1995) Complete restoration of activity to inactive mutants of *Escherichia coli* thymidylate synthase: Evidence that *E. coli* thymidylate synthase is a half-the-sites activity enzyme, *Biochemistry 34*, 1469−1474.
8. Saxl, R. L., Changchien, L.-M., Hardy, L. W., and Maley, F. (2001) Parameters affecting the restoration of activity to inactive mutants of thymidylate synthase via subunit exchange: Further evidence that thymidylate synthase is a half-of-the-sites activity enzyme, *Biochemistry 40*, 5275−5282.
9. Lorenson, M. Y., Maley, G. F., and Maley, F. (1967) The purification and properties of thymidylate synthetase from chick embryo extracts, *J. Biol. Chem. 242*, 3332−3344.
10. Agrawal, N., Hong, B., Mihai, C., and Kohen, A. (2004) Vibrationally enhanced hydrogen tunneling in the *E. coli* thymidylate synthase catalyzed reaction, *Biochemistry 43*, 1998−2006.
11. Newby, Z., Lee, T. T., Morse, R. J., Liu, Y., Liu, L., Venkatraman, P., Santi, D. V., Finer-Moore, J. S., and Stroud, R. M. (2006) The role of protein dynamics in thymidylate synthase catalysis: Variants of conserved 2′-deoxyuridine 5′-monophosphate (dUMP)-binding Tyr-261, *Biochemistry 45*, 7415−7428.
12. Phan, J., Mahdavian, E., Nivens, M. C., Minor, W., Berger, S., Spencer, H. T., Dunlap, R. B., and Lebioda, L. (2000) Catalytic cysteine of thymidylate synthase is activated upon substrate binding, *Biochemistry 39*, 6969−6978.
13. Hyatt, D. C., Maley, F., and Monfort, W. R. (1997) Use of strain in a stereospecific catalytic mechanism: Crystal structures of *Escherichia coli* thymidylate synthase bound to FdUMP and methylenetetrahydrofolate, *Biochemistry 36*, 4585−4594.
14. Spencer, H. T., Villafranca, J. E., and Appleman, J. R. (1997) Kinetic scheme for thymidylate synthase from *Escherichia coli*: Determination from measurements of ligand binding, primary and secondary isotope effects and pre-steady-state catalysis, *Biochemistry 36*, 4212−4222.
15. Hong, B., Haddad, M., Maley, F., Jensen, J. H., and Kohen, A. (2006) Hydride transfer versus hydrogen radical transfer in thymidylate synthase, *J. Am. Chem. Soc. 128*, 5636−5637.
16. Kanaan, N., Martí, S., Moliner, V., and Kohen, A. (2007) A quantum mechanics/molecular mechanics study of the catalytic mechanism of the thymidylate synthase, *Biochemistry 46*, 3704−3713.
17. Matthews, D. A., Villafranca, J. E., Janson, C. A., Smith, W. W., Welsh, K., and Freer, S. (1990) Stereochemical mechanism of action for thymidylate synthase based on the X-ray structure of the covalent inhibitory ternary complex with 5-fluoro-2′-deoxyuridylate and 5,10-methylenetetrahydrofolate, *J. Mol. Biol. 214*, 937−948.
18. Fauman, E. B., Rutenber, E. E., Maley, G. F., Maley, F., and Stroud, R. M. (1994) Water-mediated substrate/product discrimination: The product complex of thymidylate synthase at 1.83 Å, *Biochemistry 33*, 1502−1511.
19. Liu, Y., Barrett, J. E., Schultz, P. G., and Santi, D. V. (1999) Tyrosine 146 of thymidylate synthase assists proton abstraction from the 5-position of 2′-deoxyuridine 5′-monophosphate, *Biochemistry 38*, 848−852.
20. Hardy, L. W., Graves, K. L., and Nalivaika, E. (1995) Electrostatic guidance of catalysis by a conserved glutamic acid in *Escherichia coli* dTMP synthase and bacteriophage T4 dCMP hydroxymethylase, *Biochemistry 34*, 8422−8432.
21. Cook, P. F. (1991) in *Enzyme mechanism from isotope effects* (Cook, P. F., Ed.) pp 203−230, CRC Press, Boca Raton, FL.
22. Pogolotti, A. L., Weill, C., and Santi, D. V. (1979) Thymidylate synthetase catalyzed exchange of tritium from [5-^{3}H]-2′-deoxyuridylate for protons of water, *Biochemistry 18*, 2794−2798.
23. Carreras, C. W., Climie, S. C., and Santi, D. V. (1992) Thymidylate synthase with a C-terminal deletion catalyzes partial reactions but is unable to catalyze thymidylate formation, *Biochemistry 31*, 6038−6044.
24. Huang, W., and Santi, D. V. (1994) Isolation of a covalent steady-state intermediate in glutamate 60 mutants of thymidylate synthase, *J. Biol. Chem. 269*, 31327−31329.
25. Northrop, D. B. (1975) Steady-state analysis of kinetic isotope effects in enzymatic reactions, *Biochemistry 14*, 2644−2651.
26. Northrop, D. B. (1977) in *Isotope effects on enzyme-catalyzed reactions* (Cleland, W. W., O'Leary, M. H., and Northrop, D. B., Eds.) pp 122−152, University Park Press, Baltimore.
27. Northrop, D. B. (1991) Intrinsic isotope effects in enzyme catalyzed reactions, in *Enzyme mechanism from isotope effects* (Cook, P. F., Ed.) pp 181−202, CRC Press, Boca Raton, FL.
28. Cleland, W. W. (2006) Enzyme mechanisms from isotope effects, in *Isotope effects in chemistry and biology* (Kohen, A., and Limbach, H. H., Eds.) pp 915−930, Taylor & Francis, CRC Press, Boca Raton, FL.
29. Blakley, R. L. (1960) Crystalline dihydropteroylglutamic acid, *Nature 188*, 231−232.
30. Agrawal, N., Mihai, C., and Kohen, A. (2004) Microscale synthesis of isotopically labeled *R*-[6-^{x}H]-N5,N10-methylene 5,6,7,8-tetrahydrofolate as a substrate for thymidylate synthase, *Anal. Biochem. 328*, 44−50.
31. Hayatsu, H., Wataya, Y., Kai, K., and Iida, S. (1970) Reaction of sodium bisulfite with uracil, cytosine, and their derivatives, *Biochemistry 9*, 2858−2865.
32. Wataya, Y., and Hayatsu, H. (1972) Cysteine-catalyzed hydrogen isotope exchange at the 5 position of uridylic acid, *J. Am. Chem. Soc. 94*, 8927−8928.
33. Wataya, Y., and Hayatsu, H. (1972) Effects of amine on the bisulfite-catalyzed hydrogen isotope exchange at the 5 position of uridine, *Biochemistry 11*, 3583−3588.
34. Changchien, L.-M., Garibian, A., Frasca, V., Lobo, A., Maley, G. F., and Maley, F. (2000) High-level expression of *Escherichia coli* and *Bacillus subtilis* thymidylate synthase, *Protein Expression Purif. 19*, 265−270.
35. Melander, L., and Saunders, W. H. (1987) *Reaction rates of isotopic molecules*, 4th ed., Krieger, R. E., Malabar, FL.
36. Wang, L., Tharp, S., Selzer, T., Benkovic, S. J., and Kohen, A. (2006) Effects of a distal mutation on active site chemistry, *Biochemistry 45*, 1383−1392.
37. Cleland, W. W. (1980) Measurement of isotope effects by the equilibrium perturbation technique, *Methods Enzymol. 64*, 104−125.
38. Roberts, S. A., Hyatt, D. C., Honts, J. E., Changchien, L., Maley, G. F., Maley, F., and Montfort, W. R. (2006) Structure of the Y94F mutant of *Escherichia coli* thymidylate synthase, *Acta Crystallogr. F62*, 840−843.
39. Klinman, J. P., Humphriesg, H., and Voe, J. G. (1980) Deduction cf kinetic mechanism in multisubstrate enzyme reactions from tritium isotope effects, *J. Biol. Chem. 255*, 11648−11651.
40. Cook, P. F., and Cleland, W. W. (1981) Mechanistic deductions from isotope effects in multireactant enzyme mechanisms, *Biochemistry 20*, 1790−1796.
41. Cleland, W. W. (1987) Secondary isotope effectson enzymatic reactions, in *Isotopes in organic chemistry* (Buncel, E., and Lee, C. C., Eds.) pp 61−113, Elsevier, Amsterdam.
42. Kohen, A., Cannio, R., Bartolucci, S., and Klinman, J. P. (1999) Enzyme dynamics and hydrogen tunneling in a thermophilic alcohol dehydrogenase, *Nature 399*, 496−499.
43. Maglia, G., and Allemann, R. K. (2003) Evidence for environmentally coupled hydrogen tunneling during dihydrofolate reductase catalysis, *J. Am. Chem. Soc. 125*, 13372−13373.
44. Stern, M. J., and Weston, R. E. J. (1974) Phenomenological manifestations of quantum-mechanical tunneling. II. Effect on Arrhenius pre-exponential factors for primary hydrogen kinetic isotope effects, *J. Chem. Phys. 60*, 2808−2814.
45. Bell, R. P. (1980) *The tunnel effect in chemistry*, Chapman & Hall, New York,.
46. Kohen, A. (2006) Kinetic isotope effects as probes for hydrogen tunneling in enzyme catalysis, in *Isotope Effects in Chemistry and Biology* (Kohen, A., and Limbach, H. H., Eds.) pp 743−764, Taylor & Francis, CRC Press, Boca Raton, FL.
47. Francisco, W. A., Knapp, M. J., Blackburn, N. J., and Klinman, J. P. (2002) Hydrogen tunneling in peptidylglycine α-hydroxylation monooxygenase, *J. Am. Chem. Soc. 124*, 8194−8195.
48. Miller, S. M., and Klinman, J. P. (1985) Secondary isotope effects and structure-reactivity correlations in the dopamine β-monooxygenase reaction: Evidence for a chemical mechanism, *Biochemistry 24*, 2114−2127.

49. Knapp, M. J., and Klinman, J. P. (2002) Environmentally coupled hydrogen tunneling linking catalysis to dynamics, *Eur. J. Biochem. 269*, 3113−3121.
50. Nagel, Z. D., and Klinman, J. P. (2006) Tunneling and dynamics in enzymatic hydride transfer, *Chem. Rev. 106*, 3095−3118.
51. Wang, L., Goodey, N. M., Benkovic, S. J., and Kohen, A. (2006) Coordinated Effects of Distal Mutations on Environmentally Coupled Tunneling in Dihydrofolate Reductase, *Proc. Natl. Acad. Sci. U.S.A. 103*, 15753−15758.
52. Marcus, R. A. (2007) H and other transfers in enzymes and in solution: Theory and computations, a unified view. 2. Applications to experiment and computations, *J. Phys. Chem. B 111*, 6643−6654.
53. Kohen, A. (2003) Kinetic isotope effects as probes for hydrogen tunneling, coupled motion and dynamics contributions to enzyme catalysis, *Prog. React. Kinet. Mech. 28*, 119−156.

BI701363S